the plant journal

SEB SOCIETY FOR EXPERIMENTAL BIOLOGY

*The Plant Journal* (2025) **121,** e17247 doi: 10.1111/tpj.17247

# Targeted introduction of premature stop codon in plant mitochondrial mRNA by a designer pentatricopeptide repeat protein with C-to-U editing function

**Nikolay Manavski[1,*], Eslam Abdel-Salam[1], Serena Schwenkert[1], Hans-Henning Kunz[2], Andreas Brachmann[3], Dario Leister[1] and Jörg Meurer[1]**

[1]*Plant Molecular Biology, Faculty of Biology, Ludwig-Maximilians-Universität Munich, Großhaderner Street 2-4, Planegg-Martinsried 82152, Germany,*

[2]*Plant Biochemistry, Faculty of Biology, Ludwig-Maximilians-Universität Munich, Großhaderner Street 2-4, Planegg-Martinsried 82152, Germany, and*

[3]*Genetics, Faculty of Biology, Ludwig-Maximilians-Universität Munich, Großhaderner Street 2-4, Planegg-Martinsried 82152, Germany*

Received 14 October 2024; revised 11 December 2024; accepted 23 December 2024.
*For correspondence (e-mail n.manavski@biologie.uni-muenchen.de).

## SUMMARY

**RNA editing is a crucial post-transcriptional modification in endosymbiotic plant organelles, predominantly involving C-to-U conversions. Pentatricopeptide repeat (PPR) proteins play a key role in this process. To establish a system for gene expression manipulation in genetically inaccessible mitochondria, we engineered a synthetic PPR protein, dPPR-*nad7*-DYW, to induce *de novo* C-to-U editing in the *NADH dehydrogenase subunit 7* (*nad7*) mRNA of *Arabidopsis thaliana*, thereby creating a premature stop codon. This designer protein, composed of 13 P-type PPR domains, was fused with the DYW-type cytidine deaminase domain from *Physcomitrium patens* PpPPR_56 and programmed to bind a specific *nad7* mRNA segment. *In vitro* binding assays confirmed the specificity of dPPR-*nad7*-DYW for its target sequence. When expressed in Arabidopsis plants, dPPR-*nad7*-DYW achieved up to 85% editing efficiency at the target site, successfully introducing a premature stop codon in *nad7* mRNA. This resulted in reduced polysome loading of *nad7* transcripts and a phenotype characteristic of mitochondrial complex I dysfunction. RNA-sequencing revealed potential off-target editing events, albeit at lower frequencies. Our study demonstrates the successful application of an editing factor with a synthetic P-type PPR tract targeting a *de novo* editing site in plant mitochondria, achieving high editing efficiency. This approach opens new avenues for manipulating organellar gene expression and studying mitochondrial gene function in plants and other eukaryotes.**

**Keywords: mitochondria, editing, Arabidopsis, *nad7*, gene regulation, targeted downregulation, synthetic PPR proteins, posttranscriptional modification, RNA metabolism.**

## INTRODUCTION

The process of translating genetic information from DNA to protein involves an intermediary molecule, RNA, which typically mirrors the DNA sequence. However, there are instances where the RNA sequence diverges from its corresponding DNA. This alteration occurs during a post-transcriptional modification known as RNA editing, where specific RNA bases are modified relative to the original DNA sequence (Knoop, 2011; Manavski, Vicente, et al., 2021). RNA editing is particularly common in chloroplasts and mitochondria, predominantly involving C-to-U substitutions.

Pentatricopeptide repeat (PPR) proteins are crucial specificity factors for organellar RNA editing, characterized by tandem arrays of degenerate 35 amino acid repeats that form helix–loop–helix structures (Small & Peeters, 2000). These proteins are categorized into two sub-classes: P-class and PLS-class. While P-class PPRs are involved in various RNA metabolism processes, PLS-class PPRs are plant-specific and dedicated to RNA editing (Barkan & Small, 2014). Notably, PLS-class PPRs often contain an additional C-terminal extension, including the "E" (extended) motifs and "DYW" domains. The E motifs, which exhibit similarities to PPR repeats and represent straddles portions of the PPR tract and the DYW domain, are believed to be involved in either protein–protein interactions or RNA base recognition (Ruwe et al., 2019). The

DYW, which bears similarity to cytidine deaminase domains, has been proposed as the catalytic domain for organellar RNA editing. Recent *in vitro* studies and editing analyses in *Escherichia coli* have provided direct evidence of the DYW domain's editase activity, demonstrating efficient C-to-U editing by PLS-PPR proteins such as PpPPR65 and PpPPR56 from *Physcomitrium patens* (Hayes & Santibanez, 2020; Oldenkott et al., 2019).

Further understanding of these proteins comes from the development of the PPR code, which explains how PPR proteins recognize specific RNA sequences. Key findings from studies on the maize chloroplast protein PPR10 revealed that PPR proteins align parallel to RNA, with each motif contacting a single base (Pfalz et al., 2009). Specific amino acids at positions 6 and 1′ of PPR motifs, which were later described as the fifth and last positions, correlate with particular nucleotides as part of a combinatorial code that originally included S-type motifs (Barkan et al., 2012). This code was structurally validated through crystal studies of PPR10 bound to its RNA targets (Shen et al., 2016; Yin et al., 2013). The elucidation of the PPR code has not only improved our ability to predict natural PPR protein targets but also enabled the design of synthetic PPR proteins with customized RNA-binding specificities.

Building on this knowledge, researchers have developed synthetic RNA editing factors using novel pentatricopeptide repeat (PPR) protein designs. Two notable examples are the 'dsn3PLS-DYW' protein, which utilizes PLS motifs, and the 'TRX-9S-DYW' protein, based on S-type motifs (Bernath-Levin et al., 2022; Royan et al., 2021). The dsn3PLS-DYW protein was designed to target the *rpoA-78 691* editing site in *Arabidopsis thaliana* chloroplasts, achieving efficient *in planta* editing. When expressed in *E. coli*, dsn3PLS-DYW edited the *rpoA-78 691* site effectively in the presence of either MORF2 or MORF9 proteins. However, in the absence of these cofactors, the editing efficiency dropped significantly. In contrast, TRX-9S-DYW demonstrated cofactor-independent editing in *E. coli*. While these synthetic proteins show promise for advancing RNA editing technology, current research has primarily focused on known editing sites rather than completely novel targets, thus limiting their potential applications in gene expression control.

In this study, we engineered a synthetic PPR protein, designated dPPR-*nad7*-DYW, to induce *de novo* C-to-U conversion in the mitochondrial *nad7* mRNA of *A. thaliana*, thereby creating a premature stop codon. The synthetic P-type PPR tract was fused with the C-terminal DYW cytidine deaminase domain from *P. patens* PpPPR_56 and programmed to bind a specific segment of the *nad7* mRNA. dPPR-*nad7*-DYW successfully edited its target site with high efficiency in the mitochondria of stably transformed Arabidopsis plants, resulting in a Nad7-deficient phenotype. Our study demonstrates the successful application of a synthetic P-type PPR editing factor targeting a novel editing site in plants, achieving high editing efficiency and providing insights into the challenges and potential of engineered RNA editing factors for manipulating organellar gene expression.

## RESULTS

### Design of dPPR-*nad7*-DYW

The elucidation of chloroplast and mitochondrial gene function requires the precise downregulation of organelle-encoded genes. However, manipulating gene expression in plant mitochondria remains a significant challenge. In this study, we engineered a synthetic PPR protein with C-to-U editing capability to specifically induce *de novo* C-to-U conversion, thereby introducing a premature stop codon in the mitochondrial *nad7* mRNA in a targeted manner. Building on the PPR scaffold previously described (Manavski, Mathieu, et al., 2021), we designed a synthetic PPR protein comprising 13 consecutively arranged P-type PPR domains (Figure 1). The PPR tract was programmed to bind a 13-nt segment of the *nad7* mRNA, spanning the region from +168 to +180 relative to the start codon, with the amino acids at positions 5 and 35 of each PPR repeat selected according to the PPR recognition code (NS = c; TD = g; SN = a; ND = u). We fused this P-type PPR tract with the C-terminal DYW-type cytidine deaminase domain from the *P. patens* PpPPR_56 protein (amino acids 654–859), including the extension motifs, E1 and E2 (Figure 1; Figure S1). Through sequence-specific RNA binding, the PPR tract positions the DYW editing domain in close proximity to the target cytidine at position +184 within the *nad7* mRNA, with a spacer of 3 nt between the target cytidine and the binding site, enabling precise C-to-U conversion and transforming the CAA codon into a premature stop codon (UAA). To ensure mitochondrial localization, we added the mitochondrial transit peptide of the ATPase β3 subunit at the N-terminus, followed by a triple HA tag and the N-terminal domain of the maize PPR10 protein. This designer (d)PPR protein was designated dPPR-*nad7*-DYW. A truncated version of the dPPR-*nad7*-DYW protein, lacking both the DYW domain and the extension motifs, was termed dPPR-*nad7*-Δ and used as a control.

### dPPR-*nad7*-DYW introduces a premature stop codon in the *nad7* mRNA *in vivo*

First, we tested the capability of dPPR-*nad7*-DYW and dPPR-*nad7*-Δ to bind selectively to their *nad7* RNA target sequence *in vitro*. To this end, we conducted electrophoretic mobility shift assay (EMSA) experiments with purified dPPR-*nad7*-DYW and dPPR-*nad7*-Δ proteins and radiolabeled RNA probes. Both proteins successfully recognized

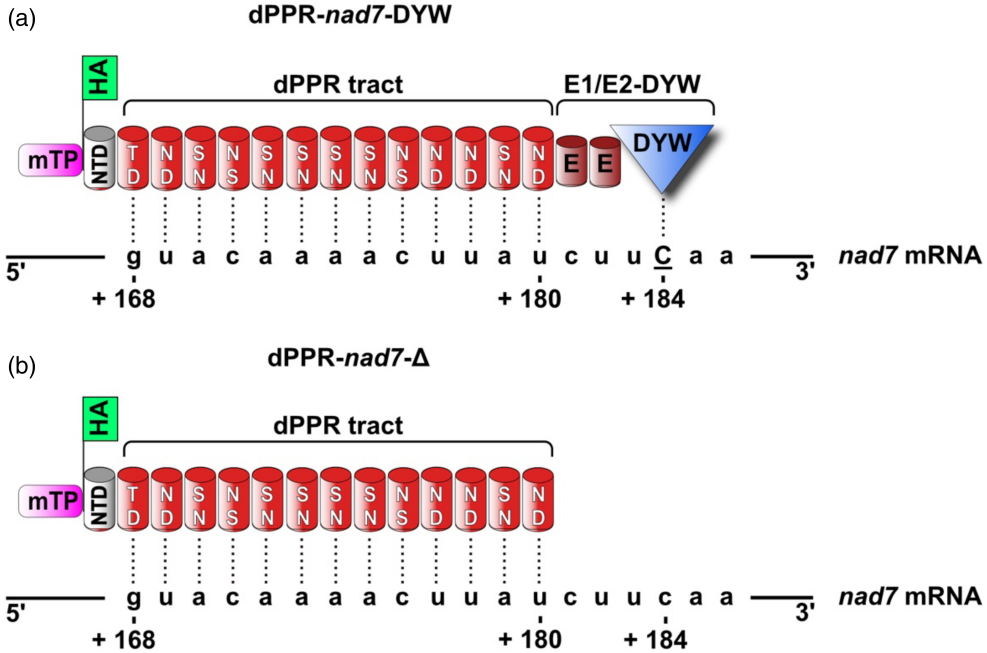


**Figure 1.** Protein design.
(a) Schematic representation of the dPPR-*nad7*-DYW protein. The PPR motifs of the PPR tract are illustrated as red cylinders, with the amino acids at positions 5 (top) and 35 (bottom) that dictate RNA binding specificity shown as capital letters. The mitochondrial transit peptide (mTP) at the N-terminus, followed by a triple HA epitope and the N-terminal domain (NTD) of the PPR10 protein, are displayed. At the C-terminus, the DYW editing domain from the *Physcomitrium patens* PpPPR_56 protein (blue triangle) along with the associated upstream extension motifs E1 and E2 (dark red cylinders labeled "E") is depicted. Based on the PPR recognition code for positions 5 and 35 (NS = c; TD = g; SN = a; ND = u), the dPPR protein was programmed to bind a 13-nucleotide region of the *nad7* mRNA, spanning positions +168 to +180 relative to the start codon. The target RNA sequence is shown beneath the dPPR *nad7*-DYW protein, with the cytidine to be edited highlighted in underlined uppercase.
(b) A truncated version, designated dPPR-*nad7*-Δ, lacking the editing domain and the two extension motifs of dPPR-*nad7*-DYW, is depicted.

their intended RNA target with strong affinity and did not bind to the control probe, demonstrating high binding specificity (Figure 2a).

Next, we assessed whether the N-terminal mitochondrial transit peptide of ATPase β3 subunit could effectively target the dPPR-*nad7*-DYW protein to mitochondria. Indeed, the GFP signals of dPPR-*nad7*-DYW-GFP overlapped with the RFP fluorescence of AOX1-RFP, a mitochondrial marker protein, in tobacco protoplasts, indicating that dPPR-*nad7*-DYW successfully targets mitochondria (Figure 2b). The merged signals showed no overlap with the chlorophyll autofluorescence, excluding mistargeting to chloroplasts.

With these prerequisites fulfilled, we proceeded to transform WT plants using the dPPR-*nad7*-DYW and dPPR-*nad7*-Δ constructs. In the T1 generation, we selected two basta-resistant dPPR-*nad7*-DYW primary transformants, along with two dPPR-*nad7*-Δ control lines (Figure 3a). In comparison to the WT, both dPPR-*nad7*-DYW mutants exhibited varying degrees of growth retardation (Figure 3a) and altered leaf morphology characteristic of mitochondrial complex I mutants at later developmental stages (Figure S2a,c). The mutant exhibiting the stronger phenotype, dPPR-*nad7*-DYW #1, produced very few viable seeds. Consequently, experiments requiring large amounts of seed or plant material, such as immunoblotting with isolated mitochondria, were conducted using the less affected dPPR-*nad7*-DYW #2 mutant, which produced more viable seeds. The expression of the dPPR-*nad7*-DYW transgene, along with the associated phenotype, has so far remained stable up to the T3 generation (Figure S2a,d). As expected, the dPPR-*nad7*-Δ control mutants, which lack the editing domain, showed no aberrant phenotype and were comparable with the WT (Figure 3a; Figure S2a). The expression of dPPR-*nad7*-DYW and dPPR-*nad7*-Δ was confirmed by immunodetection (Figure S2b).

To assess whether dPPR-*nad7*-DYW can effectively edit its target site within the *nad7* mRNA, total RNA was extracted from the dPPR-*nad7*-DYW mutants and control plants. RT-PCR was performed using *nad7*-specific primers flanking the target region. Direct sequencing of the RT-PCR products revealed a remarkably high efficiency of *de novo* C-to-U editing at the target cytidine (+184) within the *nad7* mRNA, reaching 85% in the dPPR-*nad7*-DYW #1 mutant, which exhibited the stronger phenotype (Figure 3a). Similarly, a relatively high editing efficiency of 71% was observed in the second mutant line, dPPR-*nad7*-DYW #2, which displayed a less pronounced phenotype, suggesting

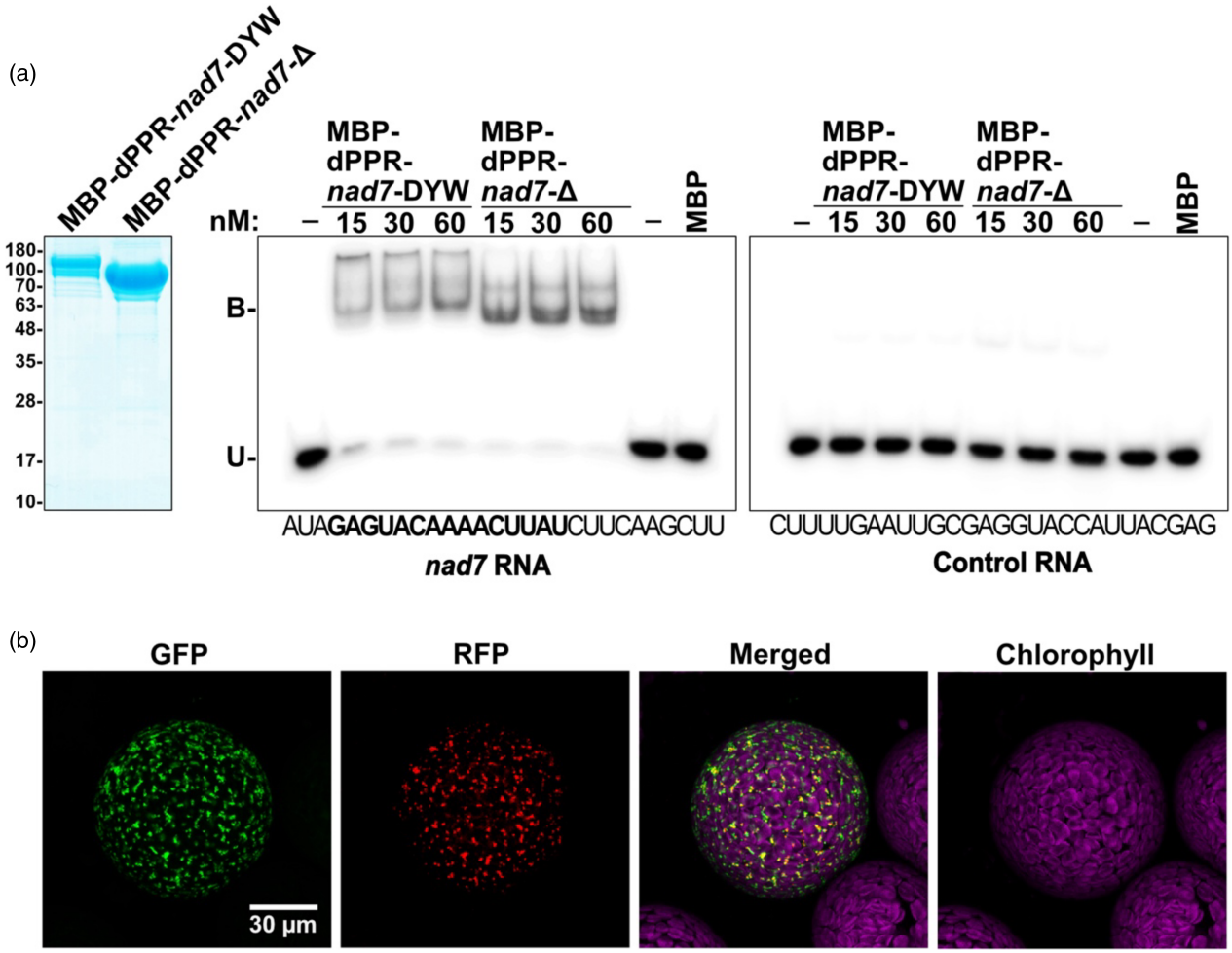


**Figure 2.** *In vitro* binding and subcellular localization.
(a) Electrophoretic mobility shift assays (EMSA) demonstrating specific *in vitro* binding of dPPR-*nad7*-DYW and dPPR-*nad7*-Δ. Increasing concentrations of dPPR-*nad7*-DYW and dPPR-*nad7*-Δ fused to maltose-binding protein (MBP) were incubated with a radiolabeled *nad7* RNA probe containing the intended binding sequence, as well as a control RNA of unrelated sequence. A reaction with MBP alone confirms that MBP does not bind RNA. The sequences of the probes are displayed below the panels, with the *nad7* target site highlighted in bold. On the left, the purified MBP-dPPR-*nad7*-DYW and MBP-dPPR-*nad7*-Δ proteins were separated by SDS-PAGE and visualized with Coomassie Brilliant Blue staining. B, bound; U, unbound.
(b) Subcellular localization of dPPR-*nad7*-DYW. Tobacco protoplasts were transiently co-transformed with dPPR-*nad7*-DYW fused to GFP and the mitochondrial marker protein AOX1 fused to RFP. GFP and RFP signals, along with chlorophyll autofluorescence, were detected using confocal microscopy. The merged image of the signals confirms the mitochondrial localization of dPPR-*nad7*-DYW.

that editing efficiency at the target cytidine correlates with the severity of the phenotype. No editing was detected in the dPPR-*nad7*-Δ control lines or WT plants. These findings confirm that dPPR-*nad7*-DYW successfully performs targeted *de novo* RNA editing.

In both mutants, the editing of the target cytidine led to conversion of the CAA (glutamine) to UAA, a stop codon. This premature stop codon terminates the translation of *nad7* at nucleotide position +184 instead of +1182 relative to the start codon, resulting in a very short, truncated polypeptide of only 61 aa instead of the full-length Nad7 protein consisting of 591 aa. Given the high percentage of editing efficiency, the majority of the *Nad7* translational products would be truncated and nonfunctional, resulting in severe impairment of NADH dehydrogenase activity in mitochondrial complex I. Indeed, an in-gel activity assay revealed that NADH oxidase activity of complex I was significantly reduced in the dPPR-*nad7*-DYW mutants compared to dPPR-*nad7*-Δ and WT plants, concomitant with stunted plant growth (Figure 3b).

The stop codon in mRNAs signals the termination of protein synthesis by instructing the ribosome to release the nascent polypeptide chain. Consequently, a premature stop codon would terminate the translation earlier, leading to reduced polysome loading of this mRNA. Therefore, we assessed whether the polysome loading of *nad7* in the

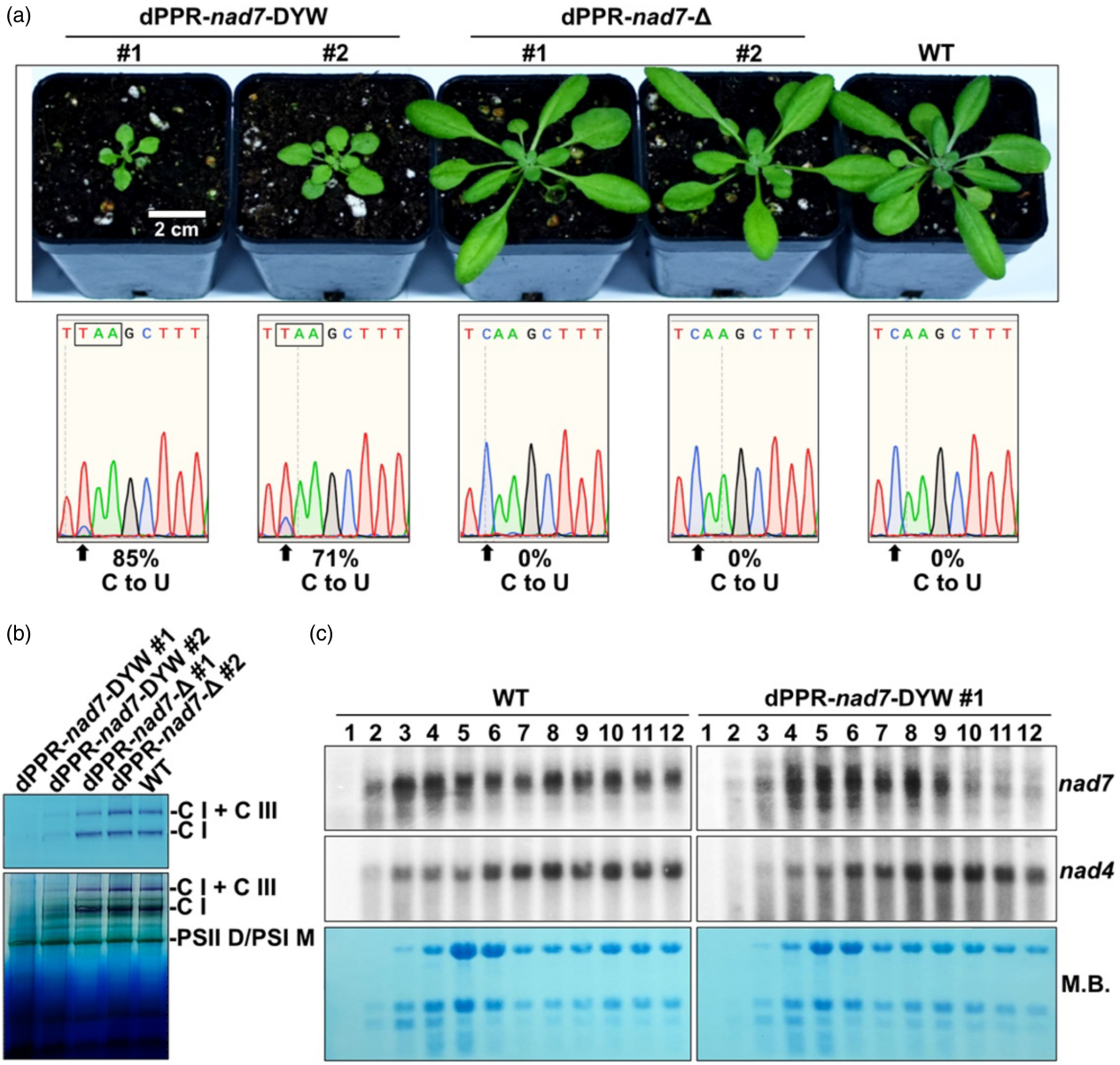


**Figure 3.** Editing efficiency and phenotype of dPPR-*nad7*-DYW.
(a) Plant phenotype of 4-week-old transgenic lines from the T3 generation expressing dPPR-*nad7*-DYW and dPPR-*nad7*-Δ compared to WT plants of the same age. The sequence chromatogram excerpts from the region containing the target cytidine are displayed beneath each genotype and demonstrate efficient C-to-U editing in the two dPPR-*nad7*-DYW mutants, with no editing events observed in WT or dPPR-*nad7*-Δ lines. The arrows indicate the position of the target cytidine, and squares highlight the created stop codons.
(b) In-gel complex I activity staining. Solubilized crude mitochondrial membrane proteins were separated by Blue native PAGE in the first dimension, and the NADH oxidase activity of complex I was assessed by incubating the gel in a NADH/NBT mixture. The bottom panel shows the unstained gel after the activity assay, while the upper panel displays the destained gel. C I, complex I; C III, complex III; PSII D, photosystem II dimer; PSI M, photosystem I monomer.
(c) Polysome loading analysis of *nad7* and *nad4* control transcripts in dPPR-*nad7*-DYW #1 and WT plants. Methylene blue (M.B.) staining of the polysome fractions (1–12) is shown.

dPPR-*nad7*-DYW mutants was affected. The RNA signals detected with a *nad7*-specific probe in the dPPR-*nad7*-DYW mutant clearly showed a shift of the peak to lighter polysome fractions, compared to the WT signals, which were present in all polysome fractions up to the heaviest ones (Figure 3c). This shift indicates that the *nad7* mRNA in the dPPR-*nad7*-DYW mutants is less loaded with polysomes, as expected. In contrast, the signal distribution of control *nad4* transcripts in dPPR-*nad7*-DYW mutants was comparable to that of the WT, indicating that the altered polysome loading in dPPR-*nad7*-DYW is restricted and specific to *nad7* transcripts.

### Off-target editing in dPPR-*nad7*-DYW mutants and molecular phenotype

To identify potential off-target sites edited by dPPR-*nad7*-DYW, we conducted RNA-Seq analysis using two biological replicates. Editing of the target cytidine (+184) in *nad7* mRNA was confirmed with a 76% C-to-U conversion rate in dPPR-*nad7*-DYW #1 mutants, along with 15 putative off-targets, all showing lower editing frequency. Alignment of these off-targets with the intended binding site of *nad7* revealed that most of the sequences upstream of the off-target cytidine moderately resembled the intended binding site in *nad7* mRNA (Figure 4).

To assess the physiological state of dPPR-*nad7*-DYW mutants, we analyzed the steady-state levels of various mitochondrial proteins in total mitochondrial extracts from dPPR-*nad7*-DYW #2, dPPR-*nad7*-Δ #2, and WT plants. Consistent with the introduction of a premature stop codon in *nad7* mRNA, Nad7 protein levels were clearly reduced in the dPPR-*nad7*-DYW #2 mutant compared to dPPR-*nad7*-Δ #2 and the WT (Figure 5a). Decreased protein levels were also observed for Nad9, which is expected since Nad7 and Nad9 are closely associated within complex I, and their accumulation is interdependent (Koprivova et al., 2010). All other tested mitochondrial proteins displayed normal or slightly elevated levels in dPPR-*nad7*-DYW #2, suggesting that the off-target editing events had no significant impact on protein levels in these mutants.

Next, we analyzed the expression of mitochondrial genes using RNA-Seq data. The heatmap (Figure 5b) shows the expression levels of all mitochondria-encoded protein-coding genes in WT and dPPR-*nad7*-Δ #1 mutants. The analysis revealed distinct differences in expression patterns between the WT and mutants, with several RNAs significantly upregulated (e.g., *nad1*, *nad4*, *nad7*, *rps4*, and *rps3*) or downregulated (e.g., *cob*, *cox2*, *atp6*, *atp8*, and *atp9*) based on an adjusted p-value <0.05 and $\log_2$ fold change >1.

Among the differentially expressed genes, *nad7* and *rps3* were significantly upregulated in the mutants. This upregulation may represent a compensatory mechanism to counteract the reduced levels of translational products caused by the premature stop codon introduced in these RNAs. Increased expression of genes encoding mitochondrial proteins could also be attributed to an elevated mitochondrial genome copy number, a phenomenon previously observed in mutants with mitochondrial respiratory failure (Ayabe et al., 2023). However, it should be noted that the observed expression variability may not

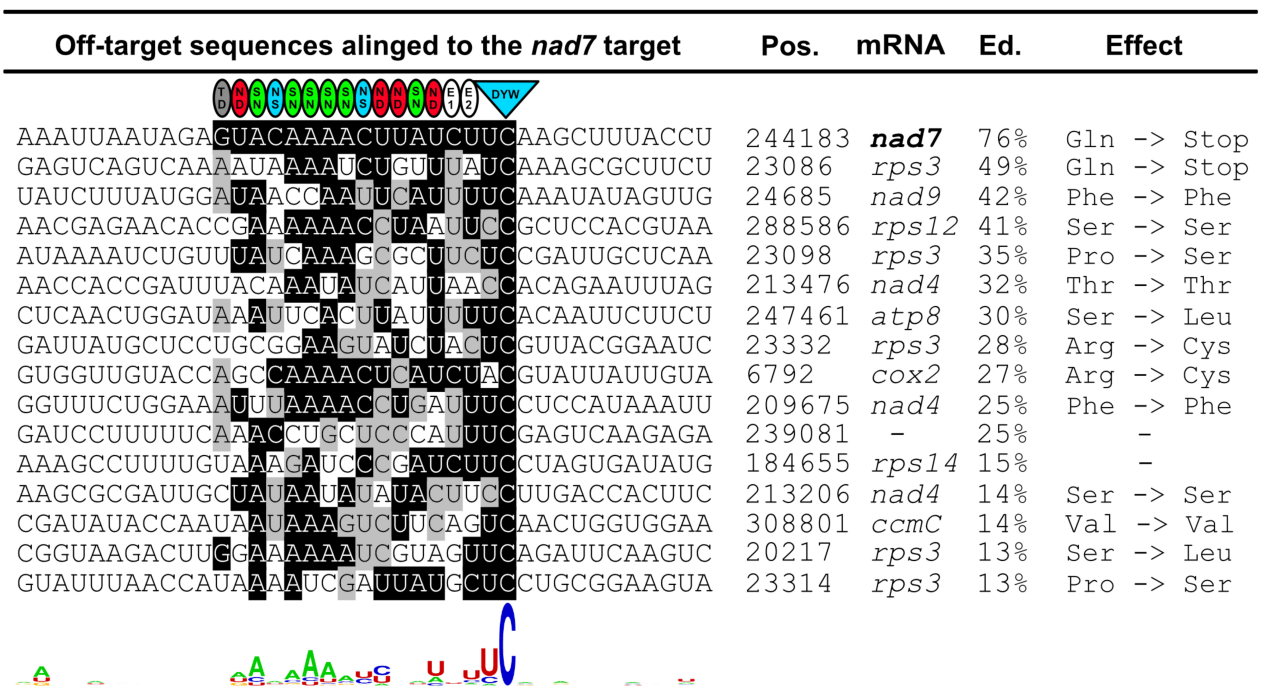


**Figure 4.** Potential off-target editing by dPPR-*nad7*-DYW.
Sequence alignment of putative off-targets. At the top, a schematic representation of dPPR-*nad7*-DYW is provided, followed by the intended binding site within the *nad7* mRNA and its flanking sequences. Below this, the sequences of potential off-target mRNAs are listed and sorted by decreasing editing efficiency (%). For each edited mRNA, the genomic position of the C-to-U conversion and its effect at the amino acid level are indicated. Bases identical to those in the *nad7* binding site and in the spacer region are highlighted in black; transition mismatches are marked in gray. A sequence logo generated using WebLogo at the bottom of the alignment highlights RNA base conservation at each position.

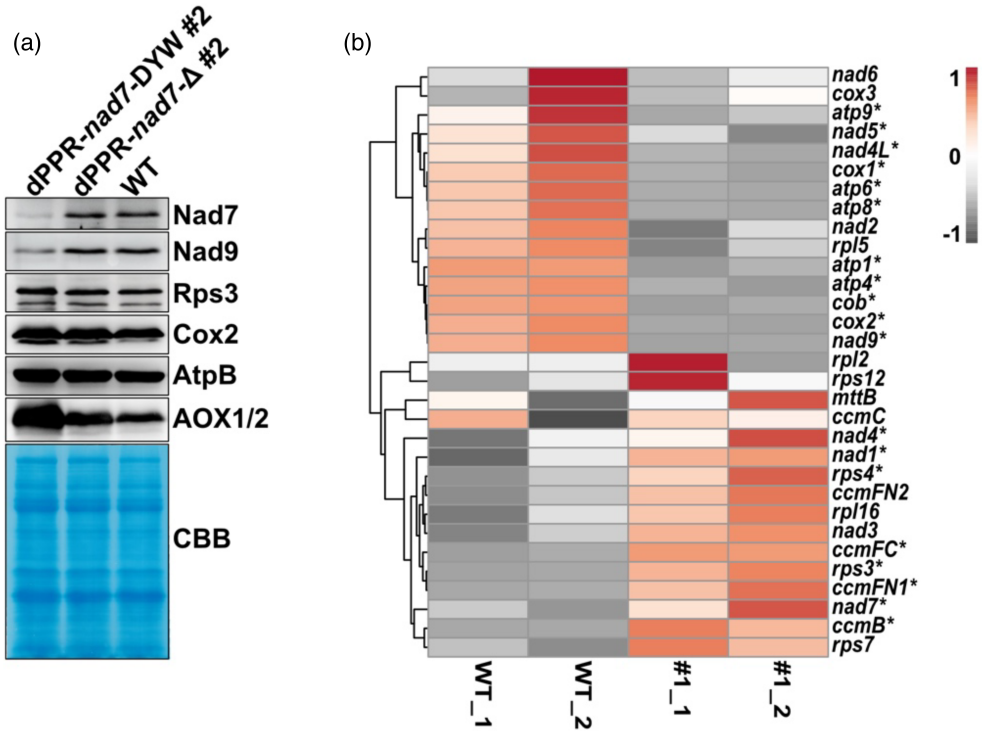


**Figure 5.** Molecular phenotype of dPPR-*nad7*-DYW mutants.
(a) Steady-state levels of different mitochondrial proteins. The antibodies used to detect the mitochondrial proteins are listed on the right. Coomassie Brilliant Blue (CBB) staining of total mitochondrial extracts served as a loading control.
(b) Heat map displaying normalized, scaled, and centered read counts of differentially expressed genes (DEGs) in dPPR-*nad7*-DYW #1 compared to WT. Upregulated genes are shown in red, and downregulated genes are represented in gray. Significantly differentially expressed genes, with an adjusted *P*-value <0.05 and $\log_2$ fold change >1, are marked with an asterisk.

solely reflect the effects of editing but could also be influenced by the severely delayed growth and development observed in the mutants compared to the WT. These physiological differences likely contribute to the altered expression profiles, highlighting the potential confounding effects of developmental stage disparities when interpreting gene-specific expression changes.

## DISCUSSION

The synthetic editing factor dPPR-*nad7*-DYW was designed to bind specifically upstream of a novel editing site at position +184 in the *nad7* mRNA, converting CAA into a premature stop codon (TAA) in stably transformed Arabidopsis plants, thereby creating a Nad7-deficient phenotype. Our EMSA experiments, editing analysis in dPPR-*nad7*-DYW mutants, and phenotypical investigations demonstrated that this goal was successfully achieved. dPPR-*nad7*-DYW represents an example of a synthetic P-type PPR editing factor targeting a *de novo* editing site. In contrast, previous synthetic PPR editing factors, such as dsn3PLS-DYW and TRX-9S-DYW, targeted pre-existing, naturally occurring editing sites (Bernath-Levin et al., 2022; Royan et al., 2021). Moreover, dPPR-*nad7*-DYW demonstrated substantially higher editing efficiency, achieving up to 85% C-to-U conversion at the target cytidine in *nad7* mRNA, compared to approximately 40% for dsn3PLS-DYW in planta and 50% for TRX-9S-DYW in bacterial systems.

While dPPR-*nad7*-DYW efficiently recognized and edited its intended target site, some potential off-targets with lower editing frequencies were also detected. Although PPR proteins are well-known for their high affinity and accuracy in RNA binding, both synthetic and endogenous PPRs exhibit some degree of off-target activity. This is expected, as absolute specificity of RNA-binding proteins is rarely achieved. The P-type PPR scaffold developed by Shen et al. (2016), which we utilized in this study, has been employed in three other *in planta* studies (Manavski, Mathieu, et al., 2021; McDermott et al., 2019; Rojas et al., 2024). In each case, some off-target activity was identified through RIP-Seq analysis, but these off-targets did not appear to have any physiologically relevant effects on the transgenic plants. Similarly, the phenotype of the dPPR-*nad7*-DYW mutants, characterized by growth retardation and altered leaf morphology, closely resembles that of other complex I mutants (Haïli et al., 2013; Koprivova et al., 2010; Sayyed et al., 2024), suggesting that the

off-target editing events have minimal or no physiological impact. This was further supported by our immunological analysis of various mitochondrial proteins that, apart from Nad7 and Nad9, accumulated to normal levels.

The specificity of synthetic P-type PPR proteins depends not only on the amino acids at positions 5 and 35 of each PPR motif but also on the length of the PPR tract. Interestingly, increasing the number of PPR motifs does not necessarily improve specificity. In fact, longer PPR tracts tend to tolerate more mismatches, as shown previously (McDermott et al., 2019). To optimize specificity, the length of the PPR tract could be shortened to 11 motifs, as studies suggest this may be less prone to nonspecific binding (Miranda et al., 2018).

Additional factors influencing binding specificity include protein concentration, RNA abundance, and the structure of the RNA target (McDermott et al., 2019). Hence, maintaining an equimolar ratio between the synthetic PPR protein and its RNA target can enhance binding specificity, while an excess of protein may lead to increased off-target activity. This underscores the necessity of screening multiple transgenic lines to identify the optimal expression levels of the synthetic PPR protein. This balance becomes even more critical when the PPR tract is fused to a catalytic effector domain, such as the DYW domain, since excessive protein concentration could favor off-target interactions. Therefore, careful experimental determination of expression levels is essential to minimize off-target effects and ensure efficient on-target editing.

With the PPR code deciphered, we are now able to design synthetic proteins to bind virtually any RNA of interest in each genetic compartment of eukaryotic cells. However, binding efficiency is influenced not only by the specific base recognition but also by the characteristics of the target sequence and its surrounding context. For example, GC-rich regions are prone to forming stable secondary RNA structures, which can inhibit RNA binding *in vitro* (Miranda et al., 2018). This is because the synthetic PPR protein must compete with the inherent base-pairing within these structures. This observation aligns with the fact that potential off-targets identified for dPPR-*nad7*-DYW were generally located in less structured, GC-poor sequences (Figure 4). Similarly, the efficiency of C-to-U conversion depends on the immediate sequence environment surrounding the editing site. In particular, the nucleotide immediately upstream of the target cytidine (referred to as the "−1" position) plays a critical role in editing efficiency (Yang et al., 2023). This should be carefully considered when selecting target sites for synthetic editing factors. In our alignment of off-target sequences, the nucleotide at position −1 was one of the most conserved and was typically occupied by a uridine (Figure 4). Previous studies have shown that purines at this position inhibit editing activity (Choury et al., 2004; Miyamoto et al., 2004; Oldenkott et al., 2019; Yang et al., 2023). Interestingly, a purine at the −1 position was identified in only one potential off-target, located at genome position 6792 within the *cox2* mRNA. Despite the presence of this inhibitory purine, the site exhibited a 25% editing frequency, suggesting that the dPPR-*nad7*-DYW is not significantly hindered by the purine in the active site.

Mitochondrial gene expression knockdown/knockout has been achieved through three primary approaches so far: ribozymes targeted to mitochondria, redesigned natural PPR proteins, and mitoTALENs. The first approach involves chimeric catalytic RNAs, consisting of a specially designed trans-cleaving hammerhead ribozyme coupled with a tRNA mimic. These constructs are transcribed in the nucleus and subsequently imported into the mitochondria via the tRNA uptake pathway. This method was successfully employed to achieve targeted cleavage of mitochondrial *atp9* mRNA in Arabidopsis, leading to its knockdown, and later applied to suppress the expression of *matR* (Sultan et al., 2016; Val et al., 2011). Although hammerhead ribozymes are generally regarded as highly specific with minimal off-target activity (Scherer & Rossi, 2003), no comprehensive off-target analysis has been performed for this approach in plant mitochondria, leaving the extent of off-target effects uncertain. Synthetic PPR proteins have also been utilized for targeted RNA cleavage in Arabidopsis mitochondria. For example, Colas des Francs-Small et al. (2018) modified the naturally occurring PPR protein RPF2 to specifically bind and cleave *nad6* mRNA. This method effectively reduced *nad6* mRNA levels, leading to a significant reduction in complex I accumulation and activity decrease in mutant plants. However, its main limitation lies in its reliance on the endogenous specificity of the original PPR protein, restricting its application to sequences closely resembling the natural binding site. Another approach, mitochondria-targeting transcription activator-like effector nucleases (mitoTALENs), combines a programmable DNA-binding domain with a nuclease domain to induce double-strand breaks at specific mitochondrial DNA (mtDNA) sites. This results in deletions of mtDNA in a stable and inheritable manner. However, this technique can inadvertently cause unintended large deletions near the target sites and trigger ectopic homologous recombination, potentially altering mitochondrial genome sequences and structure (Arimura et al., 2020; Kazama et al., 2019). A refined variant, TALEN gene-drive mutagenesis (GDM), allows for selection of mutations that confer resistance to TALEN cleavage and has been successfully used to knockout the *nad9* gene in tobacco (Forner et al., 2022). To mitigate the issue of genome instability, mitoTALENs have been further adapted in the form of mitoTALECD, where the nuclease domain is replaced with a cytidine deaminase. This approach enables precise C-to-T conversions within the mtDNA without causing deletions

or structural changes to the genome with minimal off-target effects (Nakazato et al., 2022). Nevertheless, the main drawback of mitoTALEN/CD remains the laborious and time-consuming selection process required to achieve homochondriomy. Our RNA-editing approach using designer PPR proteins offers a novel and fast alternative to the existing methods. By engineering a synthetic dPPR protein with C-to-U editing capability, we achieved precise modification of *nad7* mRNA, introducing a premature stop codon to downregulate gene expression. One of the most significant advantages of this approach is its efficiency: from design to obtaining T0 seeds, the entire process requires only about 2 months, vastly outpacing the time-intensive workflows associated with mitoTALEN-based techniques. Furthermore, due to its programmable synthetic PPR tract, our RNA-editing approach, like ribozyme and mitoTALEN/CD technologies, can target a wide range of RNA sequences. Another advantage of our approach lies in its ability to target RNA rather than DNA, offering a dynamic means of gene regulation. For example, by pairing this system with inducible promoters, it becomes possible to precisely control dPPR expression temporally, facilitating the investigation of essential genes and their roles at specific developmental stages. This strategy avoids the irreversible developmental defects often associated with constitutive knockdowns, enabling a more nuanced study of gene function in a controlled and stage-specific manner. To conclude, our method is highly effective and precise, but it does exhibit off-target effects, which, as described above, require further optimization to enhance its specificity and reliability.

In summary, this study provides a proof of concept that synthetic PPR editing factors can target *de novo* RNA editing sites with high efficiency in transgenic plants. Our design utilizes a synthetic P-type PPR tract and the DYW domain derived from *P. patens*, an organism naturally lacking RIP/MORF cofactors, making interaction with these proteins theoretically unlikely. While this suggests that our system could function independently of plant-specific cofactors like RIP/MORFs, which are essential for the activity of many endogenous PLS-type PPR proteins (Takenaka et al., 2012), further experimental validation is necessary to confirm this hypothesis. For instance, testing the dPPR-*nad7*-DYW protein in RIP/MORF-free systems, such as *E. coli*, or in RIP/MORF mutant backgrounds, could provide more concrete evidence. Nevertheless, the modular design of synthetic PPR proteins suggests they may be adaptable for use in diverse organisms, including those without plant-specific cofactors. This is supported by the successful application of PpPPR56 in heterologous systems (Lesch et al., 2022), demonstrating the broad potential of such tools. As synthetic biology continues to evolve, tools like dPPR-*nad7*-DYW will be instrumental in advancing our understanding of organelle function and improving crop resilience through targeted genetic modifications. Future studies should focus on refining these technologies to minimize off-targets while maximizing their utility in agricultural applications.

## EXPERIMENTAL PROCEDURES

### Plant material and growing conditions

All Arabidopsis plants were cultivated in soil under controlled conditions with a 12-h light (20°C)/12-h dark (18°C) cycle and a photon flux density (PFD) of 100 μmol photons $m^{-2}$ $sec^{-1}$. The Col-0 ecotype served as the wild type (WT).

*Nicotiana benthamiana* plants were grown in soil under standard greenhouse conditions with a 16-h light/8-h dark cycle at 22°C and a PFD of 200 μmol photons $m^{-2}$ $sec^{-1}$.

### Generation of transgenic plants

The coding sequence of dPPR-*nad7*-DYW was codon-optimized for *A. thaliana* (Figure S1), synthetized, and cloned into the pDONR221 by (ThermoFisher Waltham, MA, USA). The resulting construct, pDONR221:dPPR-*nad7*-DYW, was used as a template in a PCR reaction with primers Fw-ß3/Rev-DYW-trunc-stop to amplify a truncated version of dPPR-*nad7*-DYW, dPPR-*nad7*-Δ, which lacks the DYW domain (Figure S1; Table S1). The amplicon was then inserted into the pENTR/D-TOPO vector, generating the pENTR/D-TOPO:dPPR-*nad7*-Δ construct. Both pDONR221:dPPR-*nad7*-DYW and pENTR/D-TOPO:dPPR-*nad7*-Δ were subsequently recombined into the destination vector pAUL1 (Lyska et al., 2013) using LR clonase II (ThermoFisher). *Agrobacterium tumefaciens* GV3101 cells harboring the constructs pAUL1:dPPR-*nad7*-DYW and pAUL1:dPPR-*nad7*-Δ were used for floral-dip transformation of WT plants (Col-0). Primary transformants (T1) were selected by basta treatment, and transgene expression was confirmed by immunodetection with HA antibodies.

### Recombinant proteins and EMSA

The DNA sequences corresponding to the mature dPPR-*nad7*-DYW and dPPR-*nad7*-Δ proteins, both lacking the mitochondrial transit peptides (Figure S1), were amplified using the primers Fw-NTD-PPR10-*BclI*/Rev-DYW-*SalI* and Fw-NTD-PPR10-*BclI*/Rev-DYW-trunc-*SalI*, respectively (Table S1). The PCR products were digested with *BclI* and *SalI* and cloned into the *BamHI*/*SalI* sites of the pMAL-Tev vector (kindly provided by Alice Barkan, University of Oregon). Rosetta 2 (DE3) cells (Merck, Darmstadt, Germany) harboring the constructs pMAL-Tev:dPPR-*nad7*-DYW and pMAL-Tev:dPPR-*nad7*-Δ were grown to an $OD_{600}$ of 0.5, induced with 1 mM IPTG, and incubated for 3 h at 20°C with shaking (200 rpm). Cells were collected by centrifugation (5000 ***g***, 4°C, 15 min) and lysed in lysis buffer (30 mM Tris–HCl, pH 7.5, 450 mM NaCl, 5 mM β-mercaptoethanol, and cOmplete™ EDTA-free Protease Inhibitor Cocktail [Roche, Basel, Switzerland]) using sonication. Lysates were cleared by centrifugation (21 000 ***g***, 4°C, 15 min) and incubated with amylose resin (NEB, Ipswich, MA, USA) at 4°C for 1 h with rotation (10 rpm). The amylose resin was washed three times with lysis buffer and proteins were eluted in lysis buffer, containing 150 mM maltose. The proteins were further purified using an Äkta Pure system equipped with a Superdex® 200 Increase 10/300 GL column. The purification was carried out in a buffer consisting of 100 mM Tris–HCl (pH 7.5), 150 mM NaCl, 1 mM EDTA, and 5 mM β-mercaptoethanol.

EMSAs were conducted following the method described previously (Manavski, Mathieu, et al., 2021), except the gels were

frozen at −80°C during exposure to phosphor imaging screens instead of being dried.

### Subcellular localization

For subcellular localization analyses, the coding sequences of *dPPR-nad7-DYW* and *AOX1* from soybean (Uniprot: Q07185) were PCR-amplified with primers Fw-ß3/Rev-DYW and AOX-f/AOX-r (Table S1), respectively, and cloned into the pENTR/D-TOPO vector according to the manufacturer's instructions (ThermoFisher). The constructs pDONR221:dPPR-*nad7*-DYW and pENTR/D-TOPO:AOX1 were recombined into the destination vectors pB7FWG2 and pB7RWG2, respectively, using LR clonase II (ThermoFisher). Tobacco leaf infiltration and protoplast isolation were carried out as described previously (Manavski, Mathieu, et al., 2021). The confocal microscope Stellaris 5 (Leica, Wetzlar, Germany) was used to detect chlorophyll autofluorescence, eGFP, and RFP signals.

### RNA-Seq, RT-PCR, and DNA sequencing

Total RNA was extracted from 4-week-old WT and dPPR-*nad7*-DYW #1 plants using Trizol according to the manufacturer's instructions (Ambion, Austin, TX, USA). DNA contaminations were removed using the DNA-free DNA Removal Kit (ThermoFisher). RNA (10 μg) was treated with the RiboMinus™ Plant Kit (ThermoFisher) following the manufacturer's protocol. About 1 ng of RNA from each experiment was used for library generation with the NEBNext® Ultra™ II RNA Library Prep Kit according to the manufacturer's instructions (NEB). The libraries were quality controlled by analysis on an Agilent 2000 Bioanalyzer with the Agilent High Sensitivity DNA Kit (Agilent Technologies, Germany) for fragment sizes of ca. 200–500 bp. Deep sequencing (2 × 80 bp, v3 chemistry) was performed on a MiSeq sequencer (Illumina, San Diego, CA, USA) at the Genomics Service Unit (LMU Biocenter), yielding 8.2 and 9.0 million (WT replicate 1 and 2, respectively) and 8.7 and 9.8 million (dPPR-*nad7*-DYW #1 replicate 1 and 2, respectively) primary paired reads. The data are available under NCBI SRA project number PRJNA1171619.

For off-target identification, RNA-Seq reads were quality-checked and cleaned for low-quality sequences and adapter contamination using fastp v0.23.4 (Chen et al., 2018) with default parameters. The cleaned reads were then aligned to the *A. thaliana* mitochondrial genome (NC_037304.1) using BWA-MEM v0.7.18 (Li & Durbin, 2009), which generated SAM files. Potential G-to-A and C-to-U SNPs were identified with HaplotypeCaller after duplicate removal, following GATK Best Practices recommendations (McKenna et al., 2010; Van der Auwera & O'Connor, 2020). Variants were filtered to exclude those with a Phred score below 20. SNP conversion frequency was calculated by dividing the number of alternative alleles by the total read depth. Sites were considered potential off-targets only if the conversion rate was 0% in both WT samples, and G-to-A or C-to-U SNPs were detected in both mutant replicates, with a minimum read coverage of 50 in both replicates of each sample.

For differential expression analysis, aligned reads (SAM files from the off-target analysis) were assigned to genes using featureCounts v2.0.6 (Liao et al., 2014), generating a read count matrix for each gene based on the *A. thaliana* mitochondrial genome annotation. Differential expression was analyzed using DESeq2 v1.44.0 (Love et al., 2014) in R v4.4.1. Genes with an adjusted *P*-value <0.05 and $|\log_2$ fold change$|$ >1 were considered differentially expressed. A heatmap was generated using pheatmap v1.0.12, displaying scaled, normalized, and centered read counts for differentially expressed genes, with upregulated genes shown in red and downregulated genes in gray.

For RT-PCR, reverse transcription was carried out with BIORAD's (Hercules, CA, USA) iScript cDNA Synthesis Kit and DNA-free total RNA. RT-PCR was performed with the *nad7*-specific primers Fw-nad7-ORF/Rev-nad7-ORF. PCR products were gel-purified with the Wizard® SV Gel and PCR Clean-Up System (Promega, Fitchburg, WI, USA) and sequenced with the primers used for RT-PCR.

### Polysome loading analysis

Polysome loading experiments were conducted following the protocol outlined by (Barkan, 1993). RNA fractions were separated on 1.2% denaturing agarose gels containing formaldehyde and transferred onto Hybond-N+ membranes (GE Healthcare, Chicago, IL, USA) via capillary transfer in 20× SSC buffer, followed by UV crosslinking.

Radiolabeled riboprobes specific to *nad7* and *nad4* mRNAs were generated by *in vitro* transcription utilizing T7 polymerase, [$\alpha^{32}$P] UTP, and PCR products containing T7 promoter according to the manufacturer's guidelines (ThermoFisher). Blots were hybridized overnight at 68°C in PerfectHyb™ Plus hybridization buffer (Merck, Darmstadt, Germany), washed twice in buffer containing 1× SSC and 0.1% SDS, and then exposed to phosphor imaging screens.

### Blue native PAGE and immunoblot analysis

Blue native PAGE (BN PAGE) of mitochondrial respiratory complexes and subsequent complex I activity staining were performed as previously described (Vincis Pereira Sanglard & Colas des Francs-Small, 2022). The assay was conducted using 10-day-old seedlings.

For immunodetection of HA-tagged proteins, total protein was extracted from 10-day-old seedlings. Equal amounts of plant material (15 mg fresh weight) were homogenized in 100 μl of sample buffer (120 mM Tris–HCl, pH 6.8, 4% SDS, 20% glycerol, 2.5% β-mercaptoethanol, 0.01% bromophenol blue), and samples were centrifuged to remove cell debris (5 min, 21 000 ***g***, at room temperature). A 10 μl aliquot of the supernatant was then separated by SDS-PAGE on 12% Tris-Glycine gels.

For immunodetection of mitochondrial proteins, crude mitochondria were isolated as described for BN-PAGE, except that the protocol was scaled up for 1 g of plant material. Mitochondria were resuspended in sample buffer and separated by SDS-PAGE on 12% Tris-Glycine gels. Proteins were transferred onto PVDF membranes by semi-dry blotting, blocked for 1 h in 5% (w/v) skim milk prepared in TBST buffer (25 mM Tris–HCl, pH 8, 150 mM NaCl, and 0.1% [v/v] Tween 20) and incubated overnight with the primary antibodies. The membranes were subsequently washed three times with TBST buffer and then incubated with secondary antibodies in TBST buffer. Following three additional washes with TBST, signals were visualized using SuperSignal West Pico Plus Chemiluminescent Substrate (Pierce, Thermo Fisher Scientific) and analyzed with a Fusion FX7 system (PeqLab, Erlangen, Germany).

Antibodies targeting AOX1/2 (AS04 054; 1:1000), Cox2 (AS04 053A; 1:1,000), and AtpB (AS05 085; 1:5,000) were sourced from Agrisera (Vännäs, Sweden). Antibodies against Nad7 (PHY1077S; 1:1,000) were obtained from PhytoAB (San Jose, CA, USA), while monoclonal HA antibodies (H9658; 1:5,000) were acquired from Sigma-Aldrich (MO, USA). The Nad9 antibody (1:10,000) was generously provided by Hans-Peter Braun from the University of Hannover. Antibodies against Rps3 were used as described (Manavski et al., 2012). The following secondary antibodies were utilized: Goat Anti-Rabbit IgG Antibody, HRP-conjugate (Sigma-Aldrich, St. Louis, MO, USA, A9169; 1:25,000) and Goat Anti-Mouse IgG (Jackson Immuno Research, Ely, Cambridgeshire, UK, 115-035-062; 1:10,000).

## ACCESSION NUMBERS

The accession number for the *Arabidopsis thaliana* mitochondrial genome is NC_037304.1; for AOX1 from *Glycine max*, *it* is Uniprot: Q07185; and for PpPPR_56 from *Physcomitrium patens*, *it is* AB545042.1.

## AUTHOR CONTRIBUTIONS

NM conceived and designed research. NM, SS, and AB performed the experiments. NM, EA-S, H-HK, DL, and JM analyzed the data. NM wrote the manuscript with contributions from all co-authors.

## ACKNOWLEDGMENTS

This research was supported by the German Research Foundation (TR175 B07) to DL, (TR175 A03) to JM (TR175 B06) to SS, and (TR175 B09) to H-HK. Open Access funding enabled and organized by Projekt DEAL.

## CONFLICT OF INTEREST

The authors declare no conflict of interest.

## DATA AVAILABILITY STATEMENT

The data that support the findings of this study are openly available in NCBI SRA at https://www.ncbi.nlm.nih.gov/sra, reference number PRJNA1171619.

## SUPPORTING INFORMATION

Additional Supporting Information may be found in the online version of this article.

**Figure S1.** DNA and protein sequences of dPPR-*nad7*-DYW and dPPR-*nad7*-Δ. The mitochondrial transit peptide of the β3 subunit of ATP synthase is highlighted in turquoise, the HA tag in green, the N-terminal domain of PPR10 in gray, the PPR tract in red, and the DYW domain from the *Physcomitrium patens* PpPPR_56 protein along with the two extension motifs in dark blue. The amino acids at positions 5 and 35 of each PPR motif are shown in bold.

**Figure S2.** Phenotype and expression levels of dPPR-*nad7*-DYW. (a) Phenotype of 4-week-old (upper panel) and 8-week-old (lower panel) dPPR-*nad7*-DYW mutants from the T3 generation. (b) Steady state levels of dPPR-*nad7*-DYW and dPPR-*nad7*-Δ. Immunodetection was performed using total protein extracts normalized to fresh weight and HA antibodies. CBB staining of the membrane served as a loading control. (c) Phenotype of 8-week-old dPPR-*nad7*-DYW #1 siblings from the T3 generation. The persistent editing of the target cytidine (+184) in *nad7* mRNA was confirmed by sequencing the RT-PCR products, as shown below. (d) Immunodetection of dPPR-*nad7*-DYW in the plants shown in panel (c).

**Table S1.** Sequences of DNA and RNA Oligos.

**Table S2.** Off-target analysis.

## REFERENCES

**Arimura, S.I.**, **Ayabe, H.**, **Sugaya, H.**, **Okuno, M.**, **Tamura, Y.**, **Tsuruta, Y.** ***et al.*** (2020) Targeted gene disruption of ATP synthases 6-1 and 6-2 in the mitochondrial genome of *Arabidopsis thaliana* by mitoTALENs. *The Plant Journal*, **104**, 1459–1471. Available from: https://doi.org/10.1111/tpj.15041

**Ayabe, H.**, **Toyoda, A.**, **Iwamoto, A.**, **Tsutsumi, N.** & **Arimura, S.I.** (2023) Mitochondrial gene defects in Arabidopsis can broadly affect mitochondrial gene expression through copy number. *Plant Physiology*, **191**, 2256–2275. Available from: https://doi.org/10.1093/plphys/kiad024

**Barkan, A.** (1993) Nuclear mutants of maize with defects in chloroplast polysome assembly have altered chloroplast RNA metabolism. *Plant Cell*, **5**, 389–402.

**Barkan, A.**, **Rojas, M.**, **Fujii, S.**, **Yap, A.**, **Chong, Y.S.**, **Bond, C.S.** ***et al.*** (2012) A combinatorial amino acid code for RNA recognition by pentatricopeptide repeat proteins. *PLoS Genetics*, **8**, e1002910.

**Barkan, A.** & **Small, I.** (2014) Pentatricopeptide repeat proteins in plants. *Annual Review of Plant Biology*, **65**, 415–442. Available from: https://doi.org/10.1146/annurev-arplant-050213-040159

**Bernath-Levin, K.**, **Schmidberger, J.**, **Honkanen, S.**, **Gutmann, B.**, **Sun, Y.K.**, **Pullakhandam, A.** ***et al.*** (2022) Cofactor-independent RNA editing by a synthetic S-type PPR protein. *Synthetic Biology*, **7**, 1–11.

**Chen, S.**, **Zhou, Y.**, **Chen, Y.** & **Gu, J.** (2018) Fastp: an ultra-fast all-in-one FASTQ preprocessor. *Bioinformatics*, **34**, i884–i890. Available from: https://doi.org/10.1093/bioinformatics/bty560

**Choury, D.**, **Farré, J.C.**, **Jordana, X.** & **Araya, A.** (2004) Different patterns in the recognition of editing sites in plant mitochondria. *Nucleic Acids Research*, **32**, 6397.

**Colas des Francs-Small, C.**, **Vincis Pereira Sanglard, L.** & **Small, I.** (2018) Targeted cleavage of nad6 mRNA induced by a modified pentatricopeptide repeat protein in plant mitochondria. *Communications Biology*, **1**, 166.

**Forner, J.**, **Kleinschmidt, D.**, **Meyer, E.H.**, **Fischer, A.**, **Morbitzer, R.**, **Lahaye, T.** ***et al.*** (2022) Targeted introduction of heritable point mutations into the plant mitochondrial genome. *Nature Plants*, **8**, 245–256.

**Haïli, N.**, **Arnal, N.**, **Quadrado, M.**, **Amiar, S.**, **Tcherkez, G.**, **Dahan, J.** ***et al.*** (2013) The pentatricopeptide repeat MTSF1 protein stabilizes the nad4 mRNA in Arabidopsis mitochondria. *Nucleic Acids Research*, **41**, 6650–6663. Available from: https://doi.org/10.1093/nar/gkt337

**Hayes, M.L.** & **Santibanez, P.I.** (2020) A plant pentatricopeptide repeat protein with a DYW-deaminase domain is sufficient for catalyzing C-to-U RNA editing in vitro. *The Journal of Biological Chemistry*, **295**, 3497–3505.

**Kazama, T.**, **Okuno, M.**, **Watari, Y.**, **Yanase, S.**, **Koizuka, C.**, **Tsuruta, Y.** ***et al.*** (2019) Curing cytoplasmic male sterility via TALEN-mediated mitochondrial genome editing. *Nature Plants*, **5**, 722–730.

**Knoop, V.** (2011) When you can't trust the DNA: RNA editing changes transcript sequences. *Cellular and Molecular Life Sciences*, **68**, 567–586.

**Koprivova, A.**, **Francs-Small, C.C.D.**, **Calder, G.**, **Mugford, S.T.**, **Tanz, S.**, **Lee, B.R.** ***et al.*** (2010) Identification of a pentatricopeptide repeat protein implicated in splicing of intron 1 of mitochondrial nad7 transcripts. *The Journal of Biological Chemistry*, **285**, 32192–32199.

**Lesch, E.**, **Schilling, M.T.**, **Brenner, S.**, **Yang, Y.**, **Gruss, O.J.**, **Knoop, V.** ***et al.*** (2022) Plant mitochondrial RNA editing factors can perform targeted C-to-U editing of nuclear transcripts in human cells. *Nucleic Acids Research*, **50**, 9966–9983.

**Li, H.** & **Durbin, R.** (2009) Fast and accurate short read alignment with burrows-wheeler transform. *Bioinformatics*, **25**, 1754–1760.

**Liao, Y.**, **Smyth, G.K.** & **Shi, W.** (2014) featureCounts: an efficient general purpose program for assigning sequence reads to genomic features. *Bioinformatics*, **30**, 923–930. Available from: https://doi.org/10.1093/bioinformatics/btt656

**Love, M.I.**, **Huber, W.** & **Anders, S.** (2014) Moderated estimation of fold change and dispersion for RNA-seq data with DESeq2. *Genome Biology*, **15**, 550.

**Lyska, D.**, **Engelmann, K.**, **Meierhoff, K.** & **Westhoff, P.** (2013) pAUL: a gateway-based vector system for adaptive expression and flexible tagging of proteins in Arabidopsis. *PLoS One*, **8**, e53787.

**Manavski, N.**, **Guyon, V.**, **Meurer, J.**, **Wienand, U.** & **Brettschneidera, R.** (2012) An essential pentatricopeptide repeat protein facilitates 5′ maturation and translation initiation of rps3 mRNA in maize mitochondria. *Plant Cell*, **24**, 3087–3105.

**Manavski, N.**, **Mathieu, S.**, **Rojas, M.**, **Méteignier, L.V.**, **Brachmann, A.**, **Barkan, A.** ***et al.*** (2021) In vivo stabilization of endogenous chloroplast RNAs by customized artificial pentatricopeptide repeat proteins. *Nucleic Acids Research*, **49**, 5985–5997.

**Manavski, N.**, **Vicente, A.**, **Chi, W.** & **Meurer, J.** (2021) The chloroplast epitranscriptome: factors, sites, regulation, and detection methods. *Genes (Basel)*, **12**, 1121.

**McDermott, J.J.**, **Watkins, K.P.**, **Williams-Carrier, R.** & **Barkan, A.** (2019) Ribonucleoprotein capture by in vivo expression of a designer pentatricopeptide repeat protein in Arabidopsis. *Plant Cell*, **31**, 1723–1733.

**McKenna, A.**, **Hanna, M.**, **Banks, E.**, **Sivachenko, A.**, **Cibulskis, K.**, **Kernytsky, A.** ***et al.*** (2010) The genome analysis toolkit: a MapReduce framework for analyzing next-generation DNA sequencing data. *Genome Research*, **20**, 1297–1303.

**Miranda, R.G.**, **McDermott, J.J.** & **Barkan, A.** (2018) RNA-binding specificity landscapes of designer pentatricopeptide repeat proteins elucidate principles of PPR–RNA interactions. *Nucleic Acids Research*, **46**, 2613–2623. Available from: https://doi.org/10.1093/nar/gkx1288

**Miyamoto, T.**, **Obokata, J.** & **Sugiura, M.** (2004) A site-specific factor interacts directly with its cognate RNA editing site in chloroplast transcripts. *Proceedings of the National Academy of Sciences of the United States of America*, **101**, 48–52. Available from: https://doi.org/10.1073/pnas.0307163101

**Nakazato, I.**, **Okuno, M.**, **Zhou, C.**, **Itoh, T.**, **Tsutsumi, N.**, **Takenaka, M.** ***et al.*** (2022) Targeted base editing in the mitochondrial genome of *Arabidopsis thaliana*. *Proceedings of the National Academy of Sciences of the United States of America*, **119**, e2121177119.

**Oldenkott, B.**, **Yang, Y.**, **Lesch, E.**, **Knoop, V.** & **Schallenberg-Rüdinger, M.** (2019) Plant-type pentatricopeptide repeat proteins with a DYW domain drive C-to-U RNA editing in Escherichia coli. *Communications Biology*, **2**, 1–8.

**Pfalz, J.**, **Bayraktar, O.A.**, **Prikryl, J.** & **Barkan, A.** (2009) Site-specific binding of a PPR protein defines and stabilizes 5′ and 3′ mRNA termini in chloroplasts. *The EMBO Journal*, **28**, 2042–2052. Available from: https://doi.org/10.1038/emboj.2009.121

**Rojas, M.**, **Chotewutmontri, P.** & **Barkan, A.** (2024) Translational activation by a synthetic PPR protein elucidates control of psbA translation in Arabidopsis chloroplasts. *The Plant Cell*, **36**, 4168–4178.

**Royan, S.**, **Gutmann, B.**, **Colas des Francs-Small, C.** ***et al.*** (2021) A synthetic RNA editing factor edits its target site in chloroplasts and bacteria. *Communications Biology*, **4**, 545.

**Ruwe, H.**, **Gutmann, B.**, **Schmitz-Linneweber, C.**, **Small, I.** & **Kindgren, P.** (2019) The E domain of CRR2 participates in sequence-specific recognition of RNA in plastids. *The New Phytologist*, **222**, 218–229.

**Sayyed, A.**, **Chen, B.**, **Wang, Y.**, **Cao, S.K.** & **Tan, B.C.** (2024) PPR596 is required for nad2 intron splicing and complex I biogenesis in Arabidopsis. *International Journal of Molecular Sciences*, **25**, 3542.

**Scherer, L.J.** & **Rossi, J.J.** (2003) Approaches for the sequence-specific knockdown of mRNA. *Nature Biotechnology*, **21**, 1457–1465.

**Shen, C.**, **Zhang, D.**, **Guan, Z.**, **Liu, Y.**, **Yang, Z.**, **Wang, X.** ***et al.*** (2016) Structural basis for specific single-stranded RNA recognition by designer pentatricopeptide repeat proteins. *Nature Communications*, **7**, 1–8.

**Small, I.D.** & **Peeters, N.** (2000) The PPR motif - a TPR-related motif prevalent in plant organellar proteins. *Trends in Biochemical Sciences*, **25**, 45–47.

**Sultan, L.D.**, **Mileshina, D.**, **Grewe, F.**, **Rolle, K.**, **Abudraham, S.**, **Głodowicz, P.** ***et al.*** (2016) The reverse transcriptase/RNA maturase protein MatR is required for the splicing of various group II introns in Brassicaceae mitochondria. *Plant Cell*, **28**, 2805–2829. Available from: https://doi.org/10.1105/tpc.16.00398

**Takenaka, M.**, **Zehrmann, A.**, **Verbitskiy, D.**, **Kugelmann, M.**, **Hartel, B.** & **Brennicke, A.** (2012) Multiple organellar RNA editing factor (MORF) family proteins are required for RNA editing in mitochondria and plastids of plants. *Proceedings of the National Academy of Sciences of the United States of America*, **109**, 5104–5109. Available from: https://doi.org/10.1073/pnas.1208592109www.pnas.org

**Val, R.**, **Wyszko, E.**, **Valentin, C.**, **Szymanski, M.**, **Cosset, A.**, **Alioua, M.** ***et al.*** (2011) Organelle trafficking of chimeric ribozymes and genetic manipulation of mitochondria. *Nucleic Acids Research*, **39**, 9262–9274.

**Van der Auwera, G.** & **O'Connor, B.** (2020) *Genomics in the cloud: using Docker, GATK, and WDL in Terra*. Sebastopol, CA: O'Reilly Media.

**Vincis Pereira Sanglard, L.** & **Colas des Francs-Small, C.** (2022) High-throughput BN-PAGE for mitochondrial respiratory complexes. *Methods in Molecular Biology*, **2363**, 111–119.

**Yang, Y.**, **Ritzenhofen, K.**, **Otrzonsek, J.**, **Xie, J.**, **Schallenberg-Rüdinger, M.** & **Knoop, V.** (2023) Beyond a PPR-RNA recognition code: many aspects matter for the multi-targeting properties of RNA editing factor PPR56. *PLoS Genetics*, **19**, e1010733.

**Yin, P.**, **Li, Q.**, **Yan, C.**, **Liu, Y.**, **Liu, J.**, **Yu, F.** ***et al.*** (2013) Structural basis for the modular recognition of single-stranded RNA by PPR proteins. *Nature*, **504**, 168–171.